



Energy-Efficient Pedestrian Marker Light Based on Pose-Probability for Computer Vision

F. Glatzel¹, N. Müller¹, M. Waldner¹, T. Bertram¹

1: TU Dortmund University, Institute of Control Theory and Systems Engineering (RST), Dortmund, Germany

1. Abstract

The pedestrian marker lights of modern matrix headlights improve road safety at night. However, existing solutions illuminate a wide field around the pedestrian. A more precise illumination of pedestrian contours has the potential to reduce energy consumption and increase pedestrian visibility. The contribution at hand presents a novel approach for developing a luminous intensity distribution (LID) that is resized to the bounding box of pedestrians once they are detected. This LID is based on a superposition of hundreds of images of human poses, which are analyzed for the probability of each pose. Simulation-based evaluations of the new approach show a reduction in energy consumption of up to 29.7 % compared to full illumination of the pedestrian while maintaining comparable detection quality to computer vision.

Keywords: Pedestrian Marker Light, Pose-Probability

2. Introduction

Pedestrian marker lights are a safety-related innovation made possible by the advent of high-definition headlights. Modern headlight systems can detect pedestrians within the driver's field of vision and highlight them with bright areas, making the driver aware of their presence and enhancing their visibility. While the awareness of the pedestrian's presence is achieved by projecting an arrow or line in front of them, visibility is enhanced by illuminating an area around their position more brightly [1]. However, with the use of micro-LEDs in matrix headlights, the number of illuminating pixels is directly related to energy consumption, resulting in higher energy consumption for each illuminating pixel. In addition, recent research has shown that the brighter illumination of an area does not necessarily lead to better visibility of objects in that area [2]. A more precise illumination of



pedestrian contours with less excessive light is therefore interesting for reducing energy consumption and light pollution.

The contribution at hand suggests an enhanced method for selectively illuminating pedestrians. Therefore, the probability of each headlamp light ray within a pedestrian's bounding box to hit the pedestrian is examined. Based on this analysis, an adaptive LID is developed for the pedestrian within the bounding box. This so-called box LID is then adjusted to the bounding box of pedestrians once they are detected. A visualization of the resulting pedestrian marker light is shown in Fig. 1.



Figure 1: Pose-probability LID on a person in front of a white wall.

3. Light Intensity Distribution for Pose-Probability

To obtain data on the pose-probability of a pedestrian within their respective bounding box, a base dataset of pedestrians is required. The contribution at hand uses pedestrian images from the dataset [3], which contains a mix of several sub-datasets.

3.1. Data Generation from Pedestrian Images

At the beginning of data generation, each of the 890 images in the sub-dataset is reshaped to a square of 640×640 image pixels. Other resolutions are also possible. This step scales up low-resolution images to avoid inaccurate results in the final box LID and scales down high-resolution images to reduce memory usage. Each reshaped image is then processed with a YOLOv8 detection neural network to detect the bounding box coordinates of the pedestrians in the image [4]. Parallely, a YOLOv8 segmentation neural network divides the same image into two segments: the pedestrian and the surroundings, as illustrated in the first step of Fig. 2. With the detected parameters, the bounding box is then extracted from the segmented image. To normalize the data across the different images in the set, the cut-out segmented bounding box is then reshaped into a 640×640 pixel square image, as shown in the second step of Fig. 2.

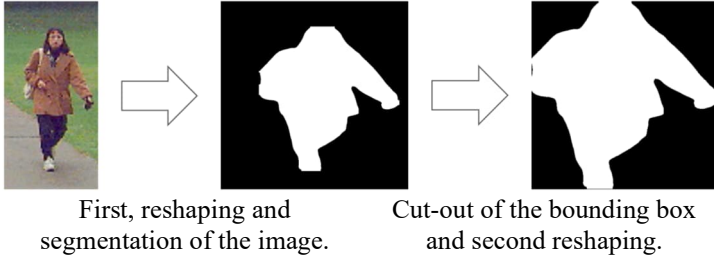


Figure 2: Data generation from pedestrian images.

Images, where none or only one of the YOLOv8 networks detect the pedestrian are labeled as unusable and excluded from the used data. Following this, 405 of the 890 photos in the sub-dataset remain usable.

3.2. Composition of the Light Intensity Distribution

After the individual images have been segmented and cut to the corresponding coordinates, the reshaped cut-outs of the images are then overlaid, resulting in a heatmap of the pose-probability of the pedestrians to their assigned bounding boxes.

To overlay the individual segmented poses, each is seen as a grayscale image that is processed as a 640×640 image matrix $I_p \in \mathbb{R}_{\geq 0, \leq 1}^{640 \times 640}$ consisting of zeros or ones. When the image pixel at position (i, j) belongs to the pedestrian then $I_p(i, j) = 1$, otherwise $I_p(i, j) = 0$. The individual matrices of segmented bounding boxes are added up and divided by the number of poses n , resulting in the average matrix $I_{\text{avg}} \in \mathbb{R}_{\geq 0, \leq 1}^{640 \times 640}$. For the position (i, j) it is:

$$I_{\text{avg}}(i, j) = \frac{1}{n} \sum_{p=1}^n I_p(i, j) \quad (1)$$

The visual image addition and elementwise division are shown in Fig. 3.

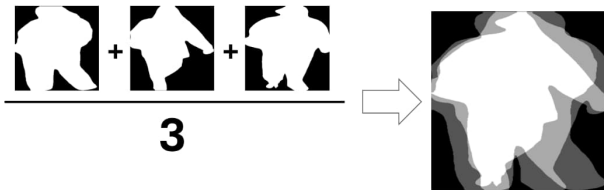


Figure 3: Illustration of a box LID composition based on three poses.

Based on the assumption that the pose-probability of a pedestrian is vertically symmetrical, I_{avg} is then overlaid with its vertically mirrored self, $I_{\text{avg, mirrored}} \in \mathbb{R}_{\geq 0, \leq 1}^{640 \times 640}$, resulting in $A_{\text{avg}} \in \mathbb{R}_{\geq 0, \leq 1}^{640 \times 640}$. For the position (i, j) it is:

$$A_{avg}(i, j) = \frac{1}{2}(I_{avg}(i, j) + I_{avg, mirrored}(i, j)) \quad (2)$$

This is equivalent to the step shown in Fig. 4a for an example image. This step effectively doubles the number of poses considered in the box LID. With all generated matrices overlaid, the resulting box LID resembles a blurred human or a snow angel, as illustrated in Fig. 4b.

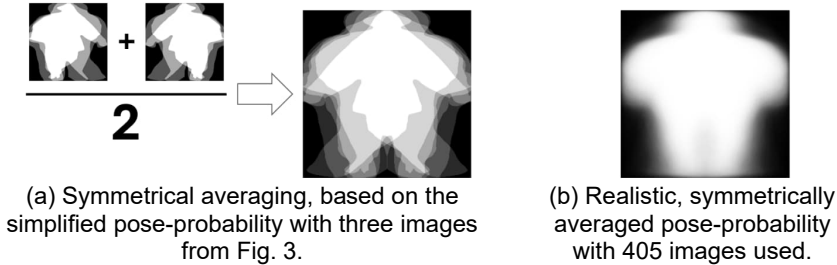


Figure 4: Visualization of symmetrical averaging and a realistic pose-probability LID.

3.3. Modifications to the Luminous Intensity Distribution

In this step, a weight function is applied to the LID, for example, to brighten darker areas or dim brighter areas selectively. This weight function is applied pixel-wise for each image pixel a_{ij} in A_{avg} , with $i, j \in \mathbb{N}$ and $i, j \leq 640$.

The simplest pixel-wise function leaves the box LID unchanged (see Fig. 5a):

$$f_1(a_{ij}) = a_{ij}. \quad (3)$$

Examples that raise the illumination of darker parts in the box LID have been evaluated, e.g., with the pixel-wise function f_2 (see Fig. 5b):

$$f_2(a_{ij}) = 1 - e^{-c \cdot a_{ij}}, \quad c \in \mathbb{R}. \quad (4)$$

The function f_3 lowers the illumination of darker areas in the box LID (see Fig. 5c):

$$f_3(a_{ij}) = a_{ij}^2. \quad (5)$$

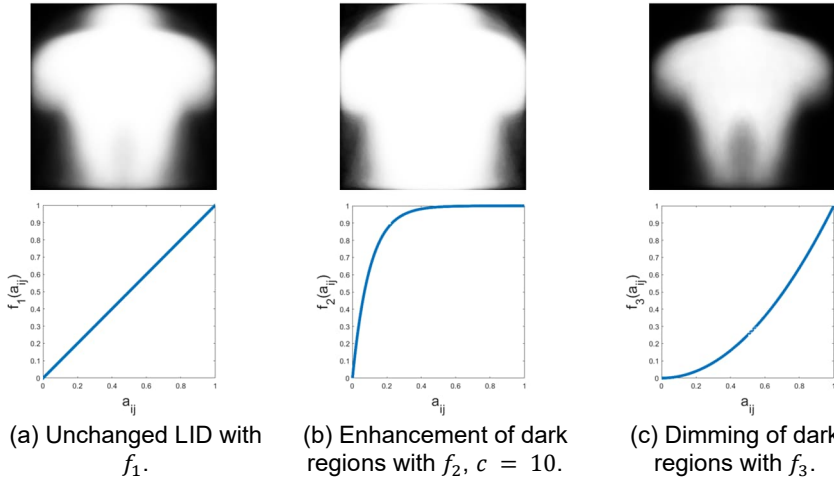


Figure 5: Visualization of f_1 , f_2 and f_3 with the corresponding graphs in the area $[0,1]$ as well as the resulting box LIDs.

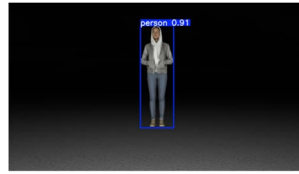
An optional additional step can apply specialized modifications to the heatmap. An example of such a special modification is the implementation of a glare-free area around the head-related area in the box LID. To avoid a potentially irritating, high-contrast cut-off line in the illumination of the pedestrian, the transition between the dimmed and the bright areas is realized with a gradually descending light intensity.

3.4. Creation of the Matrix Headlight Beam Pattern

After the creation of a pedestrian selective LID based on its pose-probability, the LID is added to the default matrix headlight beam pattern. For high-resolution headlights, this is, in principle, an overlay of the resized pedestrian LID and the base illumination, similar to an image overlap. The steps for the selective illumination of pedestrians are shown in Fig. 6. Before the selective illumination, the LID is not adapted and a pedestrian is in sight of the camera (Fig. 6a). The pedestrian is detected with a YOLOv8 network and the bounding box parameters calculated and are stored (Fig. 6b). The pre-calculated box LID (e. g. from Fig. 5a) is rescaled to the current bounding box parameters and multiplied with the box target brightness $I_{v,box}$. Then, it is added to the rest of the headlight beam pattern, which is in Fig. 6c a plain illumination with the base brightness $I_{v,base}$. Finally, the beam pattern is projected onto the scenario (Fig. 6d) by the matrix headlight.



(a) Projection of the unadopted LID.



(b) Bounding box assignment by neural network around the pedestrian.



(c) Adopted LID with scaled box LID.



(d) Projection of the pose-probability LID.

Figure 6: Composition and projection of the headlight beam pattern.

4. Evaluation

For the evaluation of the pose-probability-based LID, several LIDs are compared in six different scenarios, modeled in an Unreal Engine 5 [5] simulation.

4.1. Evaluation Setup and Criteria

A simulation of the LID is modeled in the Unreal Engine 5 for evaluation. To simplify the setup, a single camera and a single headlight are utilized. Both possess the same opening angle of 36.1° , and the number and distribution of pixels in the camera are identical to those of the projected pixels in the headlight, specifically 1920×1080 pixels. Both the camera and the headlight are positioned at the same location, 70 cm above the ground. This results in, each pixel being projected by the headlight illuminating the same pixel in the camera, and making coordinate transformations obsolete for the simulation.

For the evaluation of the pose-probability LID, six scenarios are created with a free night sky in the background and an asphalt floor. In the evaluated scenarios two different pedestrians are located in three individual positions, with every scenario featuring a single pedestrian. Positions BC-2 and DC-2 are located 25 m in front of the camera. Positions BC-1 and DC-1 are additionally shifted 15 m to the left, and positions BC-3 and DC-3 are shifted 15 m to the right. Although vertical symmetry of the pose-probability is assumed in section 3.2, the pedestrian poses are not symmetrical, especially the pedestrian pose of DC-1, DC-2 and DC-3. These values position the pedestrians at the center and along the edges of both the camera view and the headlight projection, as shown in Fig. 7.

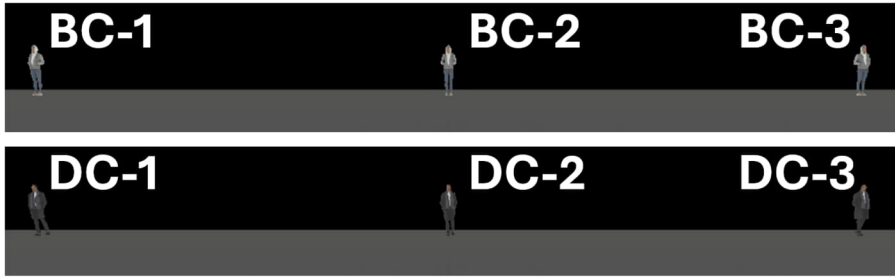


Figure 7: Visualization of the different evaluated pedestrian positions. All models are in parallel orientation, and the camera's perspective gives the illusion of a seemingly rotated orientation.

The pedestrians in BC-1, BC-2, and BC-3 are wearing light-colored clothes, resulting in high contrast with the night scenery in the background. The pedestrians in DC-1, DC-2, and DC-3 have darker clothes, resulting in a lower contrast with the background.

The confidence in detecting pedestrians in different scenarios of a YOLOv8 neural network is one of the two criteria. The second criterion is the Intersection Over Union (IoU) between the detected bounding box and the bounding box with full headlight illumination.

For the evaluation of each box LID, each scenario is first illuminated with a full illumination of all pixels, reminiscent of a base brightness $I_{v,base} = 1$, which is relative to the maximum possible headlight brightness. The pedestrian in the scenario is then detected with the YOLOv8 network. In the next step, the LID of the headlight is adapted to the scenario. The scenario is then illuminated with the adapted LID. To record the compared bounding box parameters for the evaluated LID, the YOLOv8 network recognizes the pedestrian again in the resulting image.

4.2. Compared Light Intensity Distributions

For the benchmark of the pose-probability box LID, four box LIDs are compared. The evaluated box LIDs are the pose-probability LID with the pixel-wise light function f_1 (PP), a box LID based with the pixel-wise light function f_2 with a selectively dimmed glare-free area (PPgf), a fully illuminated bounding box (HBox), and a box LID based on a 2D Gaussian bell (GBox), as shown in Fig. 8. The base brightness is set to $I_{v,base} = 0.3$ and the box brightness to $I_{v,box} = 1$. Fig. 9 shows corresponding cropped camera outputs for the box LIDs for scenario BC-2.

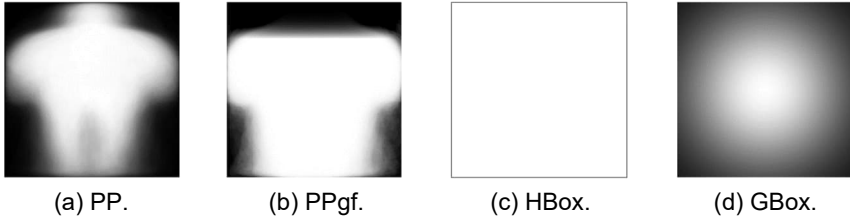


Figure 8: Compared box LIDs PP, PPgf, HBox and GBox

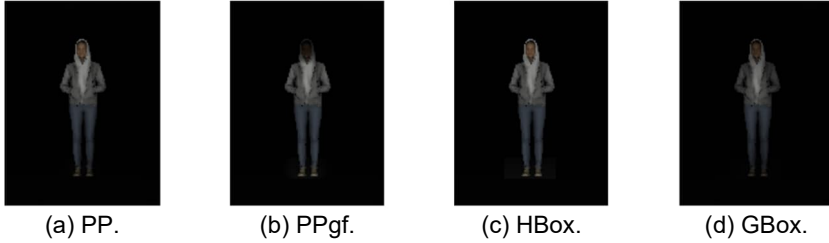


Figure 9: Camera outputs for the box LIDs PP, PPgf, HBox and GBox.

The relative energy consumption of the individual box LIDs is calculated based on the average grayscale value of each LID. This is possible because each LID is adapted to the same bounding box parameters, resulting in each LID being scaled to the same size. The individual brightness is calculated for each pixel inside the bounding box, including the base brightness of the headlamp. With that, the relative energy consumption can be compared with the relative energy consumption coefficient η :

$$\eta = \frac{1}{640 \cdot 640} \sum_{i=1}^{640} \sum_{j=1}^{640} (I_{v,\text{base}} + (I_{v,\text{box}} - I_{v,\text{base}}) \cdot a_{ij}) \quad (6)$$

Table 1 shows a comparison of the individual η values for each box LID with a base brightness $I_{v,\text{base}} = 0.3$ and a box brightness $I_{v,\text{box}} = 1$ for the brightest box pixel.

Table 1: Energy Coefficient η for each LID from (6) with a base brightness $I_{v,\text{base}} = 0.3$ and a box brightness $I_{v,\text{box}} = 1$ for the brightest box pixel.

LID	PP	PPgf	HBox	GBox
η	0.703	0.809	1	0.665

Based on the values for η , the relative energy savings can be calculated. Compared to the illumination of the full bounding box HBox, the pose-probability LID PP saves 29.7 % energy. In comparison, the glare-free LID PPgf saves 19.1 % and the Gaussian bell-based LID GBox saves 33.5 % energy.

4.3. Results

The results of the evaluation are shown in Table 2. Since the pedestrian poses are not symmetrical, as described in section 4.1, the results differ from scenario to scenario, even for the same pedestrian.

Table 2: Evaluation Results for Confidence (Conf) and Intersection over Union (IoU) in the different scenarios with different LIDs. The best values per column are printed in bold and the worst in italics.

LID	PP		PPgf		HBox		GBox	
	Conf	IoU	Conf	IoU	Conf	IoU	Conf	IoU
BC-1	0.802	0.929	0.780	0.936	0.814	0.929	0.769	0.913
BC-2	0.806	0.916	0.774	<i>0.878</i>	0.805	<i>0.880</i>	0.798	0.884
BC-3	0.822	0.911	0.787	0.920	0.819	0.926	0.794	0.934
DC-1	<i>0.561</i>	<i>0.854</i>	<i>0.612</i>	0.889	<i>0.700</i>	0.915	<i>0.389</i>	0.881
DC-2	0.755	0.937	0.764	0.926	0.758	0.930	0.584	0.903
DC-3	0.773	0.902	0.713	0.938	0.758	0.963	0.571	<i>0.872</i>

Scenarios BC-1, BC-2, and BC-3 generally have high detection quality, with a minimum confidence of 76.9 % in scenario BC-1 using GBox and a minimum IoU of 87.8 % in scenario BC-2 using PPgf. In scenario DC-1, confidence drops to 56.1 % for PP, 61.2 % with PPgf, 70.0 % with HBox, and reaches a minimum of 38.9 % with GBox. Across scenarios DC-2 and DC-3, the confidence increases to over 71 % for PP, PPgf, and HBox but remains under 59 % for GBox. In contrast to the confidence variations, the IoU remains high in these scenarios, with the minimum IoU in DC-1 with PP at 85.4 %.

In the scenarios BC-1, BC-2, and BC-3, PP and HBox result in approximately a 2 % higher absolute confidence compared to PPgf and GBox. The confidence in DC-1, DC-2 and DC-3 is lower for all LIDs. The most notable scenario is DC-1, where all LIDs exhibit a drop in confidence compared to the other scenarios. In DC-2 and DC-3, PP, PPgf, and GBox have comparable detection qualities to HBox, while GBox performs significantly worse. A possible explanation for lower detection quality is the low contrast between the pedestrian and the background.

To conclude, in scenarios with high contrast between pedestrians and the background, PP, PPgf, and GBox have the potential to maintain comparable detection quality to HBox while reducing energy consumption. In two out of the three cases evaluated, PP and PPgf remain comparable to HBox for low contrast between pedestrians and backgrounds, while GBox performs significantly worse overall in low contrast scenarios. The pose-probability LID is therefore outcompeting the 2D Gaussian bell LID in detection quality while using less

energy than illuminating the full bounding box, yet maintaining a mostly comparable detection quality.

5. Conclusion and Outlook

The presented approach shows the development of an LID that utilizes the pose-probability of a pedestrian for selective illumination. A short evaluation demonstrates the potential of a pose-probability-based LID for reducing energy consumption in the static case, saving 29.7 % in energy compared to illuminating the full bounding box when considering energy consumption within the bounding box only. Detection quality with a YOLOv8 network remains similar or slightly improved in situations with high contrast between the pedestrian and the background. In situations with low contrast between the pedestrian and the background, the pose-probability-based box LID achieves slightly worse to similar detection quality compared to the fully illuminated pedestrian. A compared box LID, based on a 2D Gaussian bell, can save 33.5 % in energy, but performs significantly worse in situations with low contrast between pedestrians and backgrounds.

A promising field for the future may be the development of the pose-probability for the LID dynamic case, as the current evaluation only describes the static case. Another interesting topic is the development of new pixel-wise light functions to reduce energy consumption further and enhance detection quality. Finally, the evaluation of additional pedestrian models, different scenarios, and more diverse backgrounds are interesting for the future of pedestrian marker lights.

6. References

- [1] Porsche (Ed.): Performance leap in light technology, <https://newsroom.porsche.com/en/2022/innovation/porsche-led-main-headlights-with-hd-matrix-beam-light-technology-30770.html>, 2022
- [2] A. Erkan, D. Hoffmann, K. Kunst, M. Peier and T. Q. Khanh: Detection conditions in urban night traffic – Does more light always mean better detection?, 15th International Symposium on Automotive Lighting, 2023
- [3] Y. Deng, P. Luo, C. C. Loy and X. Tang: Pedestrian Attribute Recognition At Far Distance, <https://mmlab.ie.cuhk.edu.hk/projects/PETA.html>, ACM MM 2014
- [4] Ultralytics (Ed.): YOLOv8, <https://docs.ultralytics.com/de/models/yolov8/>, 2025
- [5] Epic Games (Ed.): Unreal Engine 5, <https://www.unrealengine.com/en-US/unreal-engine-5>, 2025